

Plural Scattering of 20-kev Electrons in Aluminum

L. MARTON, J. AROL SIMPSON, H. A. FOWLER, AND N. SWANSON
National Bureau of Standards, Washington, D. C.

(Received October 20, 1961)

The angular and energy distribution of 20-kev electrons, scattered at very small angles ($<10^{-2}$ rad) by transmission through aluminum foils, are compared with the theory of plural inelastic scattering, under the following assumptions: (a) The probability of elastic scattering at very small angles is negligibly small in comparison with the probability of inelastic scattering. (b) Inelastic scattering occurs predominantly through sharply defined "characteristic" energy losses, whose number follows a Poisson statistical distribution. (c) The angular distribution in each loss follows a simple law: $\Phi(\theta) \propto (\theta_E^2 + \theta^2)^{-1}$. (d) The cumulative angular distribution from plural inelastic scattering is obtained

by repeated "folding" of $\Phi(\theta)$ with the angular spread of the incident beam. The angular distribution of zero-loss electrons is found to be substantially independent of the foil thickness; the normalized angular distributions of the first- and second-loss peaks are accurately fitted by the "folding" calculation; Poisson statistics gives a good approximation to the observed numbers of energy losses. The value of λ for five observations on foils of thicknesses 650–2580 Å is approximately 810 Å, independent of thickness; systematic errors in the method of observation may render this value up to 20% higher than the mean free path corresponding to the total cross section.

INTRODUCTION

PREVIOUS extensive experimentation¹ on the passage of 10–100-kev electrons through thin (~ 1000 Å) metal foils has suggested the following characteristics of the scattering phenomena:

(a) The probability of elastic scattering at very small angles ($<10^{-2}$ rad) is negligibly small in comparison with the probability of inelastic scattering. This may be a consequence of the low differential cross section for nuclear scattering in this angular range, occasioned by screening; or, the independent very-small-angle scattering from single atoms may be suppressed by coherent interference from the atoms of an extended lattice structure.

(b) Inelastic scattering occurs predominantly through sharply defined "characteristic" energy losses, whose number in a given foil follows a Poisson statistical distribution.²

(c) The angular distribution in each characteristic energy loss follows a simple law: $\Phi(\theta) \propto (\theta_E^2 + \theta^2)^{-1}$.

(d) The cumulative angular distribution resulting from plural inelastic scattering at very small angles ($<10^{-2}$ rad) is obtained by repeated "folding" of the single-scattering differential cross section with the angular spread of the incident beam.^{3,4}

The present paper contributes additional evidence for the details of this description, in regard to the passage of 20-kev electrons through aluminum foils of 600–2600-Å thickness. The more advanced features of the experiment to be reported are the following:

1. Intensity measurements are obtained on a detector which is accurately calibrated over three orders of magnitude.

2. Angular resolution of 0.25 mrad in the detector is combined with a narrow primary angular distribution (width at half-maximum ~ 1.1 mrad).

3. Angular distributions are measured for a range of accurately known foil thicknesses.

4. Energy resolution of the detector permits clear separation between the discrete-loss peaks.

These features have been individually employed in previous^{5–7} experimental work, but this is the first case in which they have been combined for a single detailed measurement.

ELEMENTS OF THE THEORY

Elastic and inelastic scattering can be regarded as statistically independent exchanges of momentum between the electron and the scattering foil. Numerous calculations⁸ have shown that the differential cross section for single-atom elastic scattering at very small angles is extremely small ($<10^{-3}$) in comparison with the probability for inelastic scattering which is observed in solids of low Z . In addition, the predominance of crystalline diffraction implies that elastic processes produce only discrete transfers of momentum, corresponding to the vectors of the reciprocal lattice. The well-known Bethe dynamical theory of diffraction suggests that in the angular region between diffraction peaks, the probability of elastic scattering is suppressed by "destructive" interference from the lattice structure. In the present experiments, attention is confined to very small angles, and therefore to zero momentum transfer in diffraction processes.⁹

¹ L. Marton, L. B. Leder, C. Marton, H. Mendlowitz, J. A. Simpson, J. A. Suddeth, and M. D. Wagner, in *Reports of the Fourth International Conference on Electron Microscopy* (Springer-Verlag, Berlin, 1960), Vol. 1, p. 281.

² H. Watanabe, *J. Phys. Soc. Japan* **11**, 112 (1956).

³ F. Leonhard, *Z. Naturforsch.* **9a**, 1019 (1954).

⁴ F. Lenz, *Z. Naturforsch.* **9a**, 185 (1954).

¹ L. Marton, L. B. Leder, and H. Mendlowitz, *Advances in Electronics and Electron Physics* (Academic Press, Inc., New York, 1955), Vol. 7, p. 183.

² A. W. Blackstock, R. H. Ritchie, and R. D. Birkhoff, *Phys. Rev.* **100**, 1078 (1955).

³ R. A. Ferrell, *Phys. Rev.* **101**, 554 (1956).

⁴ G. Wentzel, *Ann. Physik* **69**, 335 (1922).

⁹ The first-order diffraction peak in these experiments is seen at about 60×10^{-3} rad, well beyond the range $[(0-7) \times 10^{-3}]$ rad in which the angular distribution has been studied. Hence diffraction may be disregarded, except as a reduction of intensity in the transmitted beam at small angles.

Thus, we shall regard the probability of scattering through a small angle θ as the product of a probability of "no elastic momentum transfer" and the probability of inelastic scattering through an angle θ . Theoretical and experimental analysis of the statistical independence of elastic and inelastic processes, when momentum transfer occurs in elastic scattering, constitutes a separate problem.

CROSS SECTION FOR INELASTIC SCATTERING

The probability of an inelastic process with a small momentum transfer q is inversely proportional to q^2 , when the scattering is due to Coulomb forces between the incident electron and the electrons of the foil, and when account is taken of the probability of electron excitation as a result of this momentum transfer. If the electrons in the foil could be regarded as independent of one another and of the lattice, so that each electron could absorb a vanishingly small amount of recoil energy, the cross section for such a process would be proportional to $1/q^4$, according to Rutherford's law. However, the foil electrons are part of a quantum system, which absorbs in a collision only a finite amount of energy, whether its excitation be characterized as a "plasmon" or as an interband transition. In any event, we are here concerned with the observation of finite energy losses in elementary collision processes. A vanishing momentum transfer has vanishing probability of transferring a finite amount of energy to a quantum system. Therefore, the probability that a finite energy loss results from a very small momentum transfer is proportional to q^2 (the probability amplitude, which vanishes at $q=0$, is proportional to q for small q). Thus we see that the $1/q^2$ cross section arises as the product of a $1/q^4$ factor (Rutherford's law for free particles) and a q^2 factor (probability of a finite excitation with a given small q).

This theoretical argument is an essential point of the Bethe^{10,11} theory of inelastic scattering. The derivation of the result for the plasma theory has been given by Ferrell,³ and the applicability of the argument to all types of energy loss has been emphasized by Fano.¹² The differential cross section of an inelastic Coulomb interaction is given by the Born^{10,13} formula:

$$\Phi_n(q) \propto (Ze^2/q^2) |\mathcal{E}_n(q)|^2,$$

where the first factor represents the effect of Rutherford scattering and the second the probability of exciting the n th state by means of momentum transfer q . This equation may be rewritten as follows:

$$\Phi_n(q) \propto [(Ze^2)^2/q^2] |\mathcal{E}_n(q)/q|^2.$$

If we now assume that the probability amplitude $\mathcal{E}_n(q)$, for a process involving momentum transfer q , is proportional to q for small q (as is suggested by perturbation theory for both transitions between single-electron states¹⁴ and excitation of a collective oscillation¹²), the second factor will become a constant.

The resulting differential cross section may be rewritten as a function of the angle of scattering of the incident particle, making use of energy and momentum conservation. Figure 1 (which follows a similar diagram in reference 12) shows the momentum diagram for the incident particle. In the small-angle approximation (where $\sin\theta = \theta$), we have the relation

$$q^2 = (\Delta p)^2 + p^2 \theta^2 = p^2 [(\Delta p/p)^2 + \theta^2] = p^2 [\theta_E^2 + \theta^2],$$

where $\theta_E = \Delta p/p \cong \Delta E_n/2E$. Since p^2 changes by a negligibly small proportion during one scattering, we may consider it a constant. We obtain for the form of the differential cross section:

$$\Phi_n \propto 1/(\theta_E^2 + \theta^2). \quad (1)$$

In our experiments we observe a single energy loss $(\Delta E)_n$ and therefore the differential cross section given above is all we need consider. If we were to observe unresolved energy losses, the relevant angular distribution law for single scattering would be obtained by averaging this equation for values of θ_E corresponding to the various energy losses $(\Delta E)_n$ in proportion to their relative probability. The distribution so obtained, when all possible single energy losses are included, is expressed in terms of the "incoherent" scattering function of the x-ray theory.¹⁵ For the scattering by single atoms described in the Thomas-Fermi model, it is given by the Heisenberg-Bewilogua^{16,17} formula.¹⁸

Plural Scattering

Since the differential cross section for single inelastic scattering can be regarded as a probability of momentum transfer, the plural inelastic scattering process

¹⁴ Reference 10, especially pp. 332, 338-40.

¹⁵ P. M. Morse, *Physik. Z.* **33**, 443 (1932).

¹⁶ W. Heisenberg, *Physik. Z.* **32**, 737 (1931).

¹⁷ L. Bewilogua, *Physik. Z.* **32**, 740 (1931).

¹⁸ The $1/q^2$ cross section proposed here differs from the widely-quoted formula of Lenz⁸ in the following respect; in the Morse¹⁵ x-ray form for the cross section,

$$\Phi(q) = \frac{4}{\alpha h^2 q^4} [(Z-f)^2 + S],$$

the "incoherent" scattering function $S(q)$ is assumed to behave as q^2 , instead of as

$$S(q) = Z \left(1 - \frac{1}{(1+q^2\Theta/6Z)^2} \right),$$

an expression obtained from the Hartree single-atom model. In the Lenz expression, $S(q)$ is equal to $\Theta q^2/3Z$ for $q^2 \ll 6Z/\Theta$; with suitable choice of Θ , it provides a q^2 dependence at small angles with a more rapid decay at large angles. The choice of Θ in Lenz's paper is considerably smaller than the equivalent θ_E used here. However, H. Wyrwich and F. Lenz have suggested in a later paper [*Z. Naturforsch.* **13a**, 515 (1958)] that $\theta_E = \Delta E/2E$, as determined here, is indeed the pertinent parameter.

¹⁰ H. Bethe, *Ann. Physik* **5**, 325 (1930).

¹¹ H. Bethe, in *Handbuch der Physik*, edited by Greiger-Scheel, (Springer-Verlag, Berlin, 1933), Vol. 24, especially pp. 491ff.

¹² U. Fano, *Phys. Rev.* **103**, 1202 (1956).

¹³ M. Born, *Z. Physik* **38**, 803 (1926).

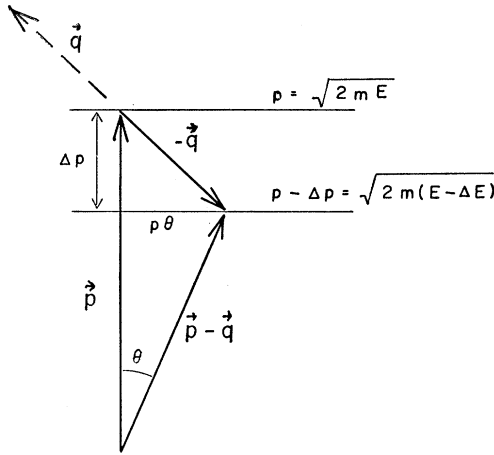


FIG. 1. Energy-momentum diagram of the primary particle; p , initial momentum; $p - \Delta p$, final momentum; q , transferred momentum; θ , angle of deflection; E , initial kinetic energy; $E - \Delta E$, final kinetic energy.

may be regarded as a random walk in transverse-momentum space, each step being weighted by the differential cross section. The law which describes this process is due to Wentzel¹⁹ and Bothe,^{20,21} and has been extensively described in the literature of plural scattering.^{22,23}

In the Wentzel representation, the probability $J(\theta; t)$ that an electron is scattered into an element of solid angle near θ (here understood to have a vector significance, corresponding to the projected momentum) after traversing a foil thickness t is composed of terms $J_N(\theta; t)$ corresponding to electrons which reach this angle by $0, 1, 2, \dots, N, \dots$ scattering processes (or steps)

$$J(\theta; t) = \sum_{N=0}^{\infty} J_N(\theta; t). \quad (2)$$

The functions J_N are separable for t and θ ,

$$J_N(\theta; t) = D_N(t)\Theta(\theta), \quad (3)$$

where

$$D_N(t) = t^N e^{-t/\lambda} / N! \quad (4)$$

and $\Theta_N(\theta)$ is a normalized angular distribution function given by

$$\Theta_N(\theta) = \int \int d^2\theta_{N-1} \int \int d^2\theta_{N-2} \cdots \int \int d^2\theta_1 \\ \times \int \int d^2\theta_0 \Theta_0(\theta_0) F(\theta_0, \theta_1) \cdots F(\theta_{N-1}, \theta). \quad (5)$$

Here the integrals are understood to be of the "folding" type in two dimensions, $\Theta_0(\theta_0)$ represents the angular distribution of the unscattered beam, and $F(\theta_1, \theta_2)$ is a two-variable representation of the differential cross

section, e.g.,

$$F(\theta_1, \theta_2) = \Phi(|\theta_1 - \theta_2|) = k / [\theta E^2 + |\theta_1 - \theta_2|^2]. \quad (6)$$

It follows from (3), (4), and (5) and from the definition of mean free path, that

$$1/\lambda = \int \int_{|\theta|=0}^{\theta_c} \Phi(\theta) d^2\theta, \quad (7)$$

(where θ_c is made finite, to give a finite total cross section) that the angular distributions $J_N(\theta; t)$ form a Poisson statistical distribution when integrated over solid angle.

$$\int \int_{|\theta|=0}^{\infty} J_N(\theta; t) d^2\theta = (t/\lambda)^N e^{-t/\lambda} / N! = P_N(t/\lambda), \quad (8)$$

for $N=0, 1, 2, \dots$.

Alternative expressions of this statistical treatment are the diffusion equation of Bothe²¹ and its Fourier-Bessel transforms^{22,23}; also the simultaneous diffusion equations of Ferrell,³ which are statistically equivalent to Eqs. (2)–(8).

APPLICATION TO EXPERIMENT

Assumptions (a)–(d) of the introduction have the following consequences for transmission scattering experiments:

(e) The assumption of zero momentum transfer in elastic processes implies that the angular distribution of emergent zero-loss electrons will be substantially independent of the thickness of the scattering foil. For a polycrystalline scatterer, the emergent angular distribution of the zero-loss electrons should be identical with that of the incident beam. This contrasts with the "diffusion" model of elastic scattering, discussed in detail by Leisegang,²⁴ which predicts a diffuse angular spread increasing with the thickness of the specimen.

(f) Poisson statistics of the inelastic scattering process requires that the discrete-loss components of the emergent beam, when integrated over solid angle, shall agree with the formula (8). If this equation is correctly applied, the argument t/λ of the Poisson function P_N , as determined from the observed statistical distribution, should prove proportional to the foil thickness t ; or λ , as determined from this argument and a measurement of foil thickness, should be the same for all foil thicknesses.

(g) The normalized angular distributions Θ_N of the discrete-loss components may be obtained by "folding" the differential cross section Φ/N times, with the initial angular distribution Θ_0 of the emergent zero-loss electrons.

CONDITIONS OF OBSERVATION

In comparing these predictions with experiment, a number of limitations inherent in the available experimental techniques must be considered.

¹⁹ G. Wentzel, *Z. Physik*, **40**, 596 (1927).

²⁰ W. Bothe, *Z. Physik*, **5**, 63 (1921).

²¹ W. Bothe, *Z. Physik*, **4**, 161 and 300 (1921).

²² G. Molière, *Z. Naturforsch.*, **3a**, 78 (1948).

²³ H. Bethe, *Phys. Rev.*, **89**, 1256 (1953).

²⁴ S. Leisegang, *Z. Physik*, **132**, 183 (1952).

5. The angular spread $\Theta_0(\theta)$ of the incident beam must not greatly exceed the half-angle θ_E of the differential cross section Φ , during the experimental tests (e) and (g). Otherwise the angular spreading due to inelastic scattering will represent only a small fraction of the initial spread, and will be difficult to separate from it. This difficulty exists in many observations which have been reported in the literature. For aluminum at 20 kev, $\theta_E = 0.37 \times 10^{-3}$ rad. In the experiments to be reported here, $\Theta_0(\theta)$ has outer limits at about 1.5×10^{-3} rad from the axis of incidence.

6. The energy analyzer must clearly accept a cone of angular width θ_E or smaller. Otherwise, the measurements of angular distribution will be smeared out—another difficulty common in the literature.

7. Unless the energy analyzer can separate the discrete-loss peaks completely from each other, difficulties of the type suggested by Ferrell³ and Watanabe⁶ may occur, in which the angular dependence of the components cannot be measured separately.

8. For the statistical comparison of paragraph (f) above, integration over the energy line shape of each peak has been shown to be desirable.² This is necessary because of the natural linewidth of the discrete-loss process, which has been studied in detail by Arai,²⁵ and which gives rise to different line shapes for the successive discrete-loss peaks. The study of these line shapes constitutes an independent experimental problem.

A common feature of energy spectrograms reported in the literature (see for example, the review article by Marton, Leder, and Mendlowitz¹) is a continuum underlying the discrete-loss spectrum. In the work to be reported, this continuum has an extremely low magnitude. The treatment of this continuum is a critical feature of the statistical comparison (f). There are a number of possible explanations for this continuum:

(i) Blackstock, Birkhoff, and Ritchie² have ascribed it to the low-energy “tail” of the thermionic distribution of primary energy, and split the continuum proportionately between the discrete-loss peaks.

(ii) If the “natural line shape” of the energy loss process is Lorentzian, the half-width of the lines will increase with N , and the continuum may be composed of overlapping tails from the discrete-loss peaks. This interpretation is encouraged by the visible changes in line shape with N in the spectrograms to be reported.

(iii) Glick and Ferrell²⁶ have proposed a “short-range” scattering process, at large angles of scattering, which would produce a continuum of this type.

(iv) It could arise from any other inelastic scattering process different from the collective type considered here.

(v) In some previous experiments the continuum

may have been associated with instrumental effects (e.g., background scattering from the analyzer baffles); the improvement in this experiment is thought to be due partly to careful electron-optical design of the decelerator and analyzer. It has not been possible to eliminate the possibility of a residual instrumental effect, however.

Since it is not possible to decide between these models on the basis of the present experimental evidence, the continuum has been subtracted from the discrete spectrum in the results to be reported here. The errors introduced by this procedure will be discussed in connection with the data.

9. The angular integration of paragraph (f) may be carried out either by using a narrow incident beam and integrating over all angles of emergence, or by using a very broad, uniform spread of angle in the primary beam, and observing at a single (central) angle of emergence. These two procedures are statistically equivalent, so far as the small-angle scattering ($< 6 \times 10^{-3}$ rad) is concerned. These techniques will be compared in the data reported here.

10. Two large-angle effects influence the evaluation of the mean free path λ from measurements of the type (f). In the Ferrell³ theory, the cutoff angle θ_c of Eq. (7), at which $\Phi(\theta)$ is expected to taper to zero, is estimated at around 12×10^{-3} or 15×10^{-3} rad. Although experimental observations by Watanabe⁶ and Marton *et al.*^{1,5,27} show a rapid experimental falloff around 18×10^{-3} or 20×10^{-3} rad, in good qualitative agreement, the cutoff limit θ_c has not been sharply predicted by theory, or accurately determined from experiment. Since the contributions to the total cross section (7) from $\theta \approx \theta_c$ region are non-negligible, this constitutes a fundamental limitation on the determination of oscillator strength for plasmon excitation [i.e., the constant multiplying the angular dependence of cross section in (1)] from mean free path.

An associated effect is the large-angle contribution to the angular integration of Eq. (7), occurring between 7×10^{-3} rad and the cutoff angle θ_c . This large-angle integration is difficult to execute experimentally; as a consequence the mean free path determined from these experiments may be up to 20% larger than the value corresponding to the total cross section for inelastic scattering. This error will be discussed in relation to the specific statistical results reported.

OBSERVATIONS

A. Instrumental Method

Recent observations in this laboratory^{5,27} with an analyzer^{28,29} which combines high angular and energy

²⁵ S. Arai, Science Repts., Tohoku Univ. First. Ser. 41, 195 (1958); 43, 121 (1959); 43, 181 (1959).

²⁶ A. J. Glick and R. A. Ferrell, Ann. Phys. (New York) 11, 359 (1960).

²⁷ L. Marton, J. Arol Simpson, J. A. Suddeth, M. D. Wagner, and H. Watanabe, Phys. Rev. 110, 1057 (1958).

²⁸ L. Marton and J. Arol Simpson, Rev. Sci. Instr. 29, 567 (1958).

²⁹ H. Mendlowitz, Rev. Sci. Instr. 29, 701 (1958).

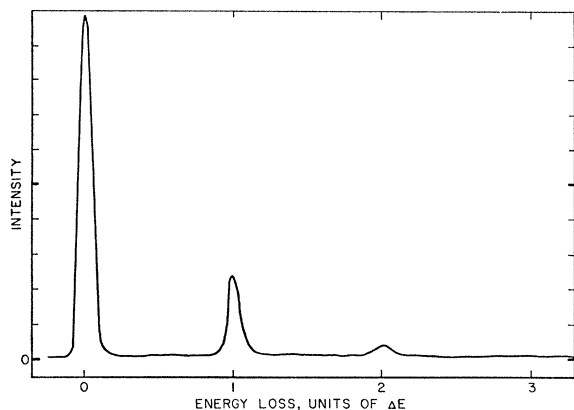


FIG. 2. Energy-loss spectrogram at $\theta=0$ for aluminum foil of thickness 650 ± 180 Å. Angular distribution of these peaks is shown in Fig. 6. Primary energy 20 kev.

resolution have confirmed and extended our earlier work^{30,31} and the observations of Leonhard⁷ and Watanabe⁶ with Möllenstedt-type³²⁻³⁵ instruments.

In this paper we shall report some new results from this high-resolution, direct-reading instrument, in which 20-kev electrons have been scattered by aluminum foils of thickness 650–2580 Å. The data are taken as energy spectrograms for fixed angles. Four such spectrograms, at zero angle, are shown in Figs. 2–5. The foil thicknesses for these examples are 650 ± 180 , 1130 ± 150 , 1710 ± 120 , and 2580 ± 100 Å. The zero-loss peaks are at the left;

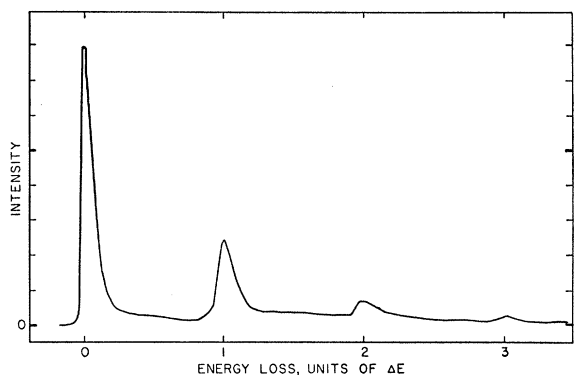


FIG. 3. Energy-loss spectrogram at $\theta=0$ for aluminum foil of thickness 1130 ± 150 Å. Angular distribution is shown in Fig. 7. Primary energy 20 kev.

the spectra consist of well-resolved discrete peaks superimposed on a very weak continuous background. There is slight evidence of weak 10-v loss peaks accompanying the dominant 15-v ones; these are thought from the

³⁰ L. Marton, J. Arol Simpson, and T. F. McCraw, *Rev. Sci. Instr.* **26**, 855 (1955).

³¹ J. Arol Simpson, T. F. McCraw, and L. Marton, *Phys. Rev.* **104**, 64 (1956).

³² G. Möllenstedt, *Optik* **5**, 499 (1949).

³³ H. Boersch, *Naturwissenschaften* **35**, 26 (1948).

³⁴ H. Boersch, *Optik* **5**, 436 (1949).

³⁵ W. Kleinn, *Optik* **11**, 226 (1954).

work of Powell and Swan³⁶ to be associated with the surface-loss³⁷ phenomenon, rather than with the prominent bulk-loss oscillation of the plasma³⁸ model.

Energy analysis is performed in our measurements by decelerating the electrons from 20 kev to 300 ev, passing them through the field of a Siegbahn-type analyzer magnet, post-accelerating, and recording intensity with a phosphor-photomultiplier detector, which is run as part of a logarithmic photometer circuit.³⁹ This detector compresses a large range of signal into a small output

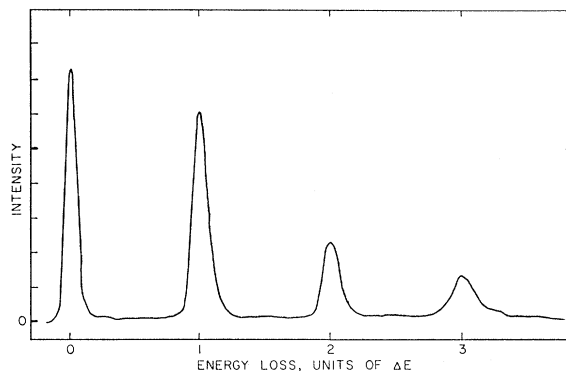


FIG. 4. Energy-loss spectrogram at $\theta=0$ for aluminum foil of thickness 1710 ± 120 Å. Angular distribution is shown in Fig. 8. Primary energy 20 kev.

deflection, enabling spectra with a large range of intensity to be recorded rapidly with no loss of detail. The chart records of output are converted back by a photometrically-established calibration curve, to give a linear intensity spectrum. The detector may also be operated in linear mode; that is, with constant photomultiplier voltage, the output signal being amplified by

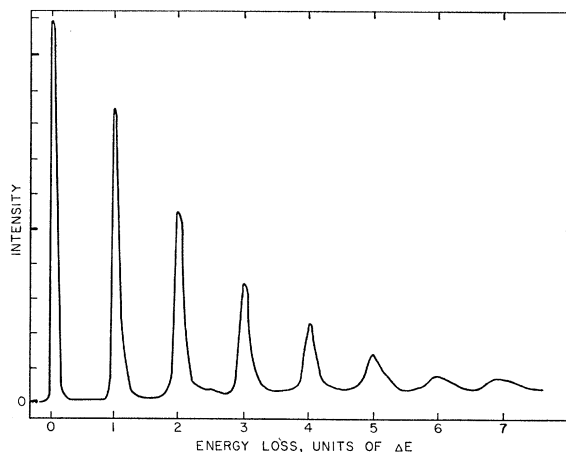


FIG. 5. Energy-loss spectrogram at $\theta=0$ for aluminum foil of thickness 2580 ± 100 Å. Angular distribution is shown in Fig. 9. Primary energy 20 kev.

³⁶ C. J. Powell and J. B. Swan, *Phys. Rev.* **115**, 869 (1959).

³⁷ R. H. Ritchie, *Phys. Rev.* **106**, 874 (1957).

³⁸ D. Pines and D. Bohm, *Phys. Rev.* **85**, 338 (1952).

³⁹ R. E. Bell and R. L. Graham, *Rev. Sci. Instr.* **23**, 301 (1952).

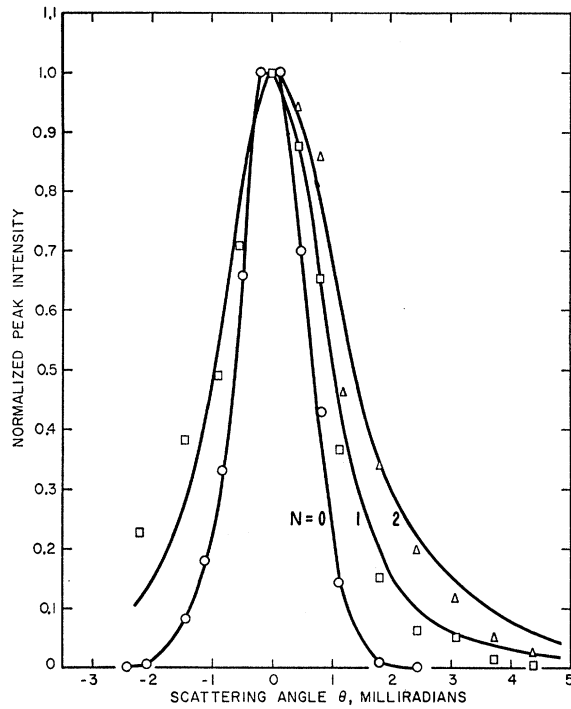


FIG. 6. Normalized angular distributions of the zero-loss, first-loss, and second-loss peaks of Fig. 2. Points are experimental peak heights, normalized at $\theta=0$. Smooth zero-loss curve is fitted to zero-loss points. First-loss and second-loss curves are computed by folding the Bethe-Ferrell differential cross section with the experimental zero-loss and first-loss points, with $\theta_E=0.350 \times 10^{-3}$ and 0.370×10^{-3} rad (see Appendix).

a direct coupled circuit having a 2-msec response time. No appreciable differences have been found between the two modes of operation; the spectra obtained from the two methods agree within about $\pm 3\%$, over 2 orders of magnitude of range. Since the logarithmic mode enables low-intensity details to be recorded simultaneously with high-intensity ones, it is generally preferred when the angular dependence of spectra with both weak and strong peaks is to be measured. The cartograph plots shown in earlier publications^{5,31} have been compiled from series of such logarithmic-mode spectra, taken at a series of increasing scattering angles.

B. Angular Distribution of the Zero-Loss Peak

In Figs. 6-9 are shown the measured angular distributions of the zero-loss, first-loss, second-loss, and (in one case) the third-loss peaks for these spectra. The data are normalized to a value of one at zero angle. The points shown are the intensities-at-maximum of the individual peaks; if energy areas of the peaks are used instead, similar results are obtained, since there is very little change of energy spread in the peaks over the small angular range (less than 7 mrad) covered. These data are similar to some published by Watanabe.⁴⁰

⁴⁰ H. Watanabe, J. Phys. Soc. Japan 16, 912 (1961).

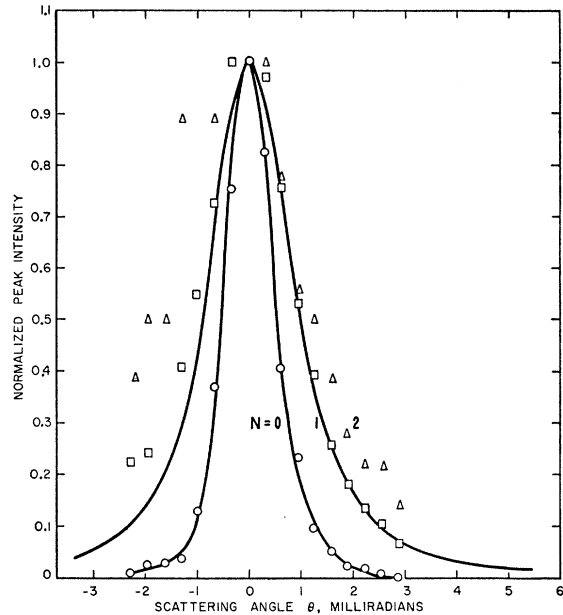


FIG. 7. Normalized angular distributions of the zero-loss, first-loss, and second-loss peaks of Fig. 3. Points are experimental peak heights, normalized at $\theta=0$. Smooth zero-loss curve is fitted to zero-loss points. First-loss curve is computed by folding this with the Bethe-Ferrell differential cross section, with $\theta_E=0.350 \times 10^{-3}$ rad, corresponding to $\Delta E=14.0$ ev.

The innermost curve in each plot is a smooth function approximating the experimental points for the zero-loss, "elastic" peak. It will be noted that the angular width

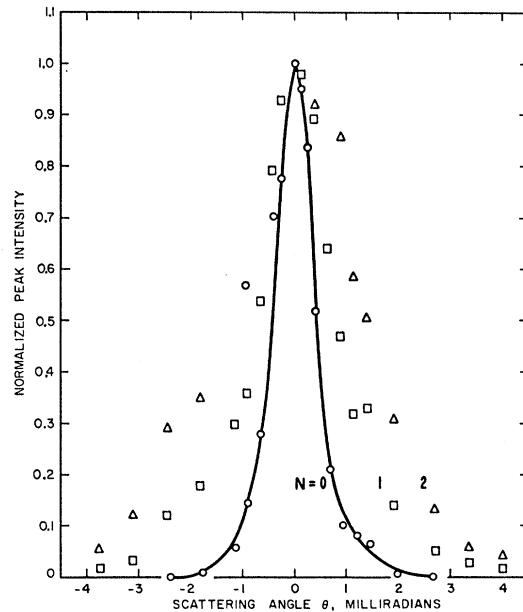


FIG. 8. Normalized angular distributions of the zero-loss, first-loss, and second-loss peaks of Fig. 4. Points are experimental peak heights. Smooth zero-loss curve is fitted to zero-loss points. First- and second-loss curves have not been calculated for this specimen, because of normalization errors in the first- and second-loss experimental points (see text).

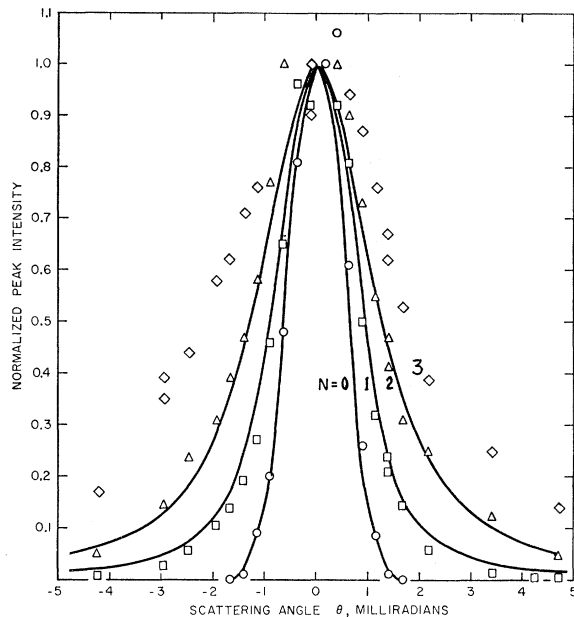


FIG. 9. Normalized angular distributions of the zero-loss, first-loss, second-loss, and third-loss peaks of Fig. 5. Points are experimental peak heights. Smooth zero-loss curve is fitted to zero-loss points. First- and second-loss curves are computed from the zero-loss and first-loss points, respectively, by folding with the Bethe-Ferrell cross section, with $\theta_E = 0.370 \times 10^{-3}$ rad, corresponding to $\Delta E = 14.8$ ev.

of this function does not increase systematically with thickness of foil; in fact, the narrowest angular distribution has been observed for the 1710 Å specimen. This observation is taken to suggest point (e) above, namely that the angular distribution is that characteristic of a central peak, identical with that of the incident beam. The variations which are observed between these specimens are interpreted as small shifts in the incident angular distribution.

The sharp zero-loss angular distribution recorded in Fig. 8 shows that the angular acceptance of the energy analyzer is close to its estimated value of 0.25 mrad. Were this not the case, the sharp central maximum could not be so clearly distinguished.

A direct comparison of this emergent angular elastic distribution with that of the incident beam is difficult, because of the very large difference in intensity between the incident and emergent beams. The outer limits of the incident beam are found to agree (within a rather large error, of about ± 0.3 mrad) with the limits of the emergent beam seen here, however, if the incident beam is observed by the detector with no foil or holder present in the system.

The narrow angular spread in this incident beam is achieved with a Steigerwald⁴¹ type gun, having a cored oxide-cathode emitter of the Uyeda type,⁴² and an additional 0.25 mm defining aperture between the gun

⁴¹ F. W. Braucks, *Optik* **15**, 242 (1958).

⁴² K. Ando, O. Kamigaito, Y. Kamiya, S. Takahashi, and R. Uyeda, *J. Phys. Soc. Jap.* **14**, 180 (1959).

and the aluminum specimen. The condition of the cathode (small emitting area), and its position relative to the aperture of the grid electrode are found to be critical for obtaining a narrow angular distribution.

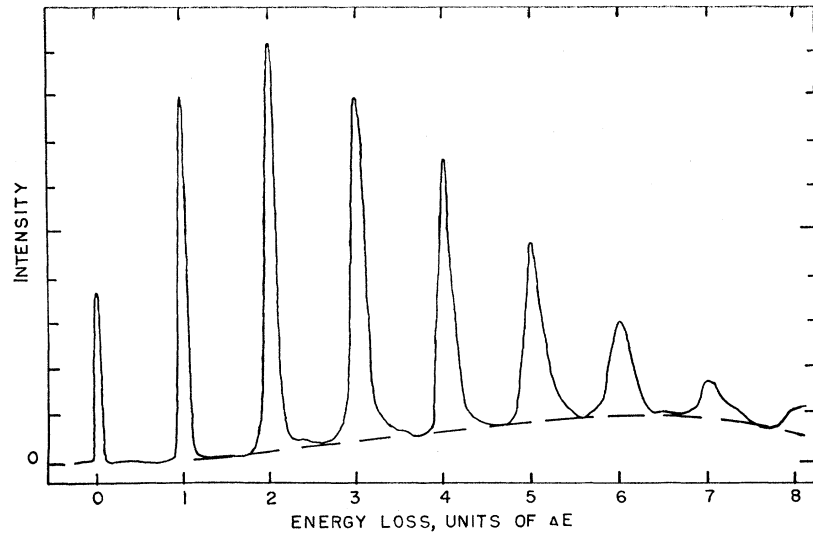
C. Angular Distribution of the Discrete-Loss Peaks

It is immediately seen from these plots that the first, second, \dots , etc., discrete-loss experimental points form a family of curves of increasing spread. The smooth first-loss curves shown have been calculated by a numerical folding of the smooth zero-loss approximation function with the Ferrell differential cross section. The details of this calculation are described in the Appendix. Similarly, the second-loss curves have been calculated by a folding of a smooth approximation function for the first-loss points (not shown) with the same cross section. Two slightly different values of θ_E have been used in calculation of these curves (see Appendix), but it is not possible to depart far from the parametric value $\theta_E = \Delta E/2E$ without obtaining a folding integral which is either much wider or much narrower than the corresponding experimental points.

Encouragingly good agreement between the calculated curves and the measured points is noted, even though no correction has been made for the finite angular acceptance of the analyzer. Several details of agreement emphasize the general correctness of the theoretical description. Both the calculated curve and the experimental points for the first-loss peak show a long tail at large θ , which is totally absent in the zero-loss angular distribution. This is a consequence of the long $1/\theta^2$ tail of the Bethe-Ferrell differential cross section, which extends out to some 20 mrad before cutoff (in this integration procedure the folding has been cut off at about 8 mrad, since the angular-distribution measurements were carried out only to about 6 mrad). In addition, the spreading of the first-loss peak at small angles is well fitted by the value of θ_E set by the Bethe-Ferrell theory; this is the only parameter in the differential cross section. This experimental fit appears more accurate than the earlier ones of Ferrell.³

Thus we see that the predictions of the Wentzel folding-integral theory are accurately borne out by experiment, if the differential cross section for inelastic scattering is chosen to be that given by the Bethe-Ferrell theory. The folding-integral calculations have been carried out only on data where an experimentally significant comparison between the curves and the experimental data could be obtained. (In Fig. 8 the zero-loss angular distribution has an extremely narrow central peak—so narrow that the loss peaks in this region show irregular variations of intensity, apparently as a result of the detector slipping to one side or other of the central maximum. Under these conditions it is difficult to obtain a good normalization for the angular distribution points, and these cannot be considered to

FIG. 10. Energy-loss spectrogram at $\theta=0$ for the specimen of Fig. 5, taken with wide primary angular distribution (see text). Dashed curve is fitted to the minima between peaks; the continuum beneath this curve is subtracted for statistical comparison with the Poisson distribution.



have as good internal consistency as those in the other plots. The same type of angular spreading can be observed in these points, however.)

It will be noted that the angular effects described by the folding integral theory are independent of foil thickness, when normalized angular functions are used; this is in full agreement with the predictions of the Wentzel theory.

D. Comparison with Poisson Statistics

To complete the comparison with plural-scattering theory, it is now desirable to compare the statistical population of the discrete-loss peaks with the Poisson formula. The angular spreading associated with inelastic scattering has an important effect on the statistical distribution of electrons among the various loss peaks. For example, the spectrogram of Fig. 10 has been taken on the same specimen as the spectrogram of Fig. 5; however, in Fig. 10 the angular spread of the incident beam is much larger. In contrast with the zero-loss angular spread shown in Fig. 9, the zero-loss beam used to obtain Fig. 10 extends from -3.5 mrad to $+3.5$ mrad, with a flat maximum of about 2-mrad width. This spread approximates the limiting case of wide angular distribution (half-width of the incident beam much greater than $2\theta_E$) which was discussed in paragraph (g) above. The zero-loss, first-loss, and second-loss peaks are seen to be much less strongly weighted than in the spectrogram of Fig. 5. In addition, a weak continuum appears under the discrete spectrum at large values of energy loss, as indicated by the dashed line. This continuum, it will be noted, is less pronounced in all of the spectrograms taken with narrow incident angular distribution.

If the area under the dashed curve is subtracted from the spectrum, and the remaining areas of the peaks integrated graphically by planimeter, the results may be compared with a Poisson distribution, as is shown

in Fig. 11. (This treatment differs from that of Blackstock, Ritchie, and Birkhoff² only in the interpretation of the continuum.) A high degree of fit is obtained with a Poisson function: $P_N(t/\lambda) = (t/\lambda)^N e^{-t/\lambda} / N!$ of argument $t/\lambda = 3.2$. It will be noted that this is an eight-point fit.

The zero-angle spectrogram of Fig. 5 is not in agreement with this Poisson function, of course. In principle, however, we may weight the zero-angle spectrum by the integrated solid-angle spread of each peak. The calculation is indicated graphically in Fig. 13. Assuming the angular distributions of Fig. 9 to extend with cylindrical symmetry, the products of the angular distributions $J_N(\theta)$ with $|\theta|$ are shown as functions of $|\theta|$. The curves are expected to approach asymptotically the dashed line, of slope 1, at small $|\theta|$. The areas under these curves should correspond to the weighting factors for

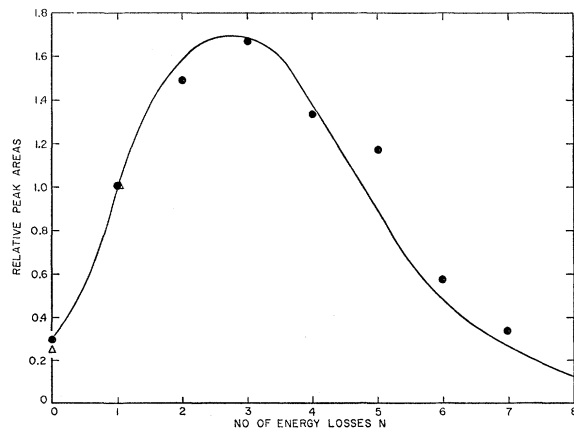


FIG. 11. Poisson distribution of the energy-loss peaks in Fig. 10: ● areas of the peaks, with dashed continuum subtracted; Δ areas of the zero-loss and first-loss peak of Fig. 5, weighted by the angular calculation of Fig. 13 (see text); solid line, the continuous function $(t/\lambda)^N e^{-t/\lambda} / \Gamma(N+1)$ [which coincides with $P_N(t/\lambda)$ for integral values of N], with argument $t/\lambda = 3.20$.

the solid-angle spread of each peak. It will be noted that the zero-loss function is sharply cut off at about 1.4 mrad from the axis of the scattered beam, whereas the first-loss peak has a large-area tail extending out beyond 5 mrad. It appears from these measurements that the second-loss peak does not have a finite tail; certainly it cannot be determined with any accuracy beyond 6 mrad. Hence, the weighting factors can be estimated accurately only for the zero-loss and first-loss peaks. If they are so measured, and the areas of the Fig. 5 spectrogram multiplied by them, the two triangles of Fig. 11 are obtained, in good agreement with the Poisson distribution obtained from the wide incident beam.

This small-angle effect has not been explicitly considered in previous experimental comparisons^{2,43-48} of characteristic-loss spectra with Poisson statistics. The most successful measurement of this type to date, by Blackstock, Ritchie, and Birkhoff, has tacitly assumed that the scattering is one dimensional; however, the success of their comparison is probably a result of the fact that the incident beam had a wide angular spread, and possibly that the angular acceptance of the detector was also rather large. In measuring the areas of the peaks, these authors assumed that the weak continuum underlying the discrete-loss spectrum was composed of long tails on the discrete-loss peaks, and divided its area accordingly. This tends to give a higher value of argument in the Poisson function derived to fit the data. These authors have not demonstrated as detailed a fit to the Poisson distribution as is shown here. In their case t/λ is not determined to better than $\pm 15\%$. Hence, the comparison reported here differs in several critical respects from that of Blackstock, Ritchie, and Birkhoff and is felt to represent a more rigorous approach.

E. Determination of Mean Free Path

An alternative method of displaying this data, which emphasizes the good agreement with a Poisson distribution, is shown in Fig. 12. From Eq. (8), if

$$J_N(t) = \int \int_{|\theta|=0}^{\infty} J_N(\theta; t) d^2\theta$$

is the area of the N -loss peak integrated over all angles of scattering, then

$$N! J_N(t) = (t/\lambda)^N e^{-t/\lambda}, \quad (9)$$

or

$$\log(N! J_N) = N \log(t/\lambda) - t/\lambda. \quad (10)$$

Thus a semilog plot of $N! J_N$ as a function of N should be a straight line of slope $\log(t/\lambda)$. This is indeed found

to be the case, in Fig. 12. The straight line for $t/\lambda = 3.20$ fits closely the small-error points from $N=0$ to $N=4$; the dashed line for $t/\lambda = 3.33$ includes the points $N=5$ to $N=7$ better, and shows that the statistical error in determining this slope is not the limiting feature of the measurement, since the two values of t/λ agree within 4%. Perceptibly poorer agreement with the experimental points will be obtained for any slope outside the range $3.20 < t/\lambda < 3.33$.

If this value of t/λ can be combined with an accurate measurement of foil thickness, a mean free path for the inelastic process may be determined. The thickness of the specimen used for the measurements of Figs. 9-13 is 2580 ± 100 A, giving a mean-free-path value of 810 ± 60 A, if the value $t/\lambda = 3.20$ is used.

As has been indicated in (f), the same value should be obtained for all foil thicknesses, if the mean free path does not vary from specimen to specimen. The angular distribution curves of Figs. 6-8 may be used to weight the zero-loss and first-loss peaks of the zero-angle spectrograms in Figs. 2-4, giving the following table of mean free paths:

TABLE I. Comparison of mean free path for Al foils of various thickness.

Foil thickness, t (angstroms)	t/λ from Poisson function	λ , mean free path (angstroms)	Limits of error
650 ± 180	0.75 (2-point fit)	870	± 200
1130 ± 150	1.4 (2-point fit)	810	± 110
1710 ± 120	2.2 (2-point fit)	780	± 80
2580 ± 100	3.2 (8-point fit)	810	± 60

The data reported in this table are for a set of specimens which exhibited low background continuum, and for which the thicknesses are reliably known. These are not isolated examples of the Poisson-distribution fitting procedure, however. A number of 5- and 7-point fits to Poisson distributions, similar to the data of Figs. 10 and 12, have been obtained for specimens exhibiting larger background continuum, and for which the thicknesses were less accurately known.

It will be seen that the values obtained from the spectra of Figs. 2, 3, and 4 agree with the more reliable value of Fig. 10, within the limits of error of the individual observations. The primary limiting factor in these observations is the determination of specimen thickness, which has been performed by the Fizeau-Tolansky^{49,50} multiple-beam reflection interferometer method. Since this method has certain systematic limitations in the measurement of film thicknesses, which have not been described in the literature, it is appropriate to describe it briefly.

⁴³ E. Sternglass, *Nature* **178**, 1387 (1956).

⁴⁴ G. Ruthemann, *Ann. Physik* **437**, 113 (1948).

⁴⁵ H. Friedmann, *Naturwissenschaften* **41**, 569 (1954).

⁴⁶ H. Friedmann, *Z. Naturforsch.* **11a**, 373 (1956).

⁴⁷ H. Friedmann, *Fortschr. Physik* **V**, 2, 51 (1957).

⁴⁸ W. Lang, *Optik* **3**, 233 (1948).

⁴⁹ S. Tolansky, *Multiple-Beam Interferometry* (Oxford University Press, New York, 1948).

⁵⁰ S. Tolansky, *Surface Microtopography* (Interscience Publishers, Inc., New York, 1960).

F. Measurement of Specimen Thickness

It should be remembered that these experiments are performed on self-supporting aluminum foils [which are evaporated on a stripping layer of evaporated rocksalt, or Victawet 35B (sodium lauryl and octyl phosphate)] and transferred to the specimen holder by floating on a water surface. A number of samples from the areas adjacent to the scattering specimen are picked up on microscope slides, some of which are clean, and others of which are coated with an optically opaque mirror of evaporated aluminum. These specimens are then silvered by the Tolansky prescription, and the step at the edge of each specimen is measured in the reflection interferometer. As Tolansky has shown, this type of step can be measured with considerable accuracy; here we find an interferometer error of about ± 20 A. Indeed, the interferometer measurements are not found to be the limiting factor; a more important question is whether the step height of the silver coating corresponds exactly to the thickness of the aluminum specimen. In this connection it has been observed that the specimens picked up on a glass backing exhibit a lower measurement of thickness (by an irregular amount, ranging up to three or four hundred A) than those picked up on the aluminum backing. There are several possible interpretations of this discrepancy, the most plausible of which appears to be a different sticking probability for the first monolayer of silver on glass and aluminum surfaces. Under this interpretation the thickness measurements with the aluminum backing should have the minimum systematic error, since silver is evaporated on aluminum at each side of the step. These are the measurements which are quoted in the mean-free-path

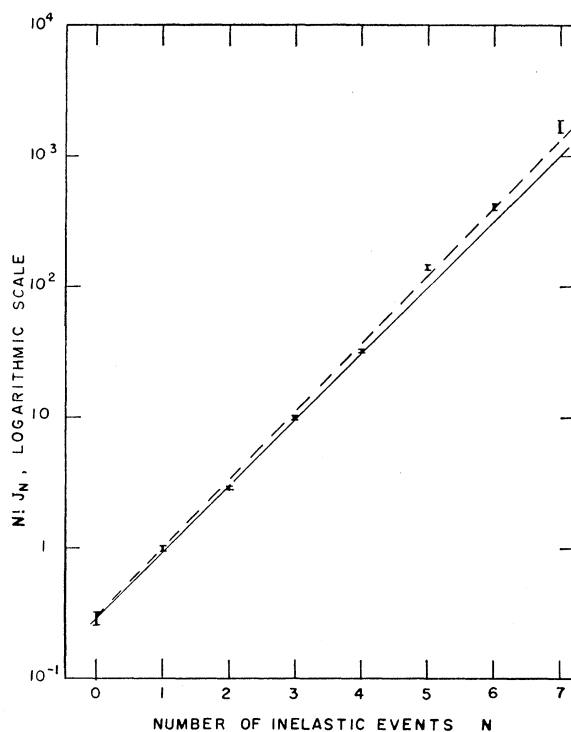


FIG. 12. Logarithmic representation of the Poisson distribution in Fig. 11; $N!J_n$ is shown as a function of N , where J_n is the area of the N th loss peak in Fig. 10: solid line, $P_N(t/\lambda)$ for $t/\lambda=3.20$; dashed line, $P_N(t/\lambda)$ for $t/\lambda=3.33$.

table (Table I); the errors are the maximum departures of the thickness sample measurements from the mean values.

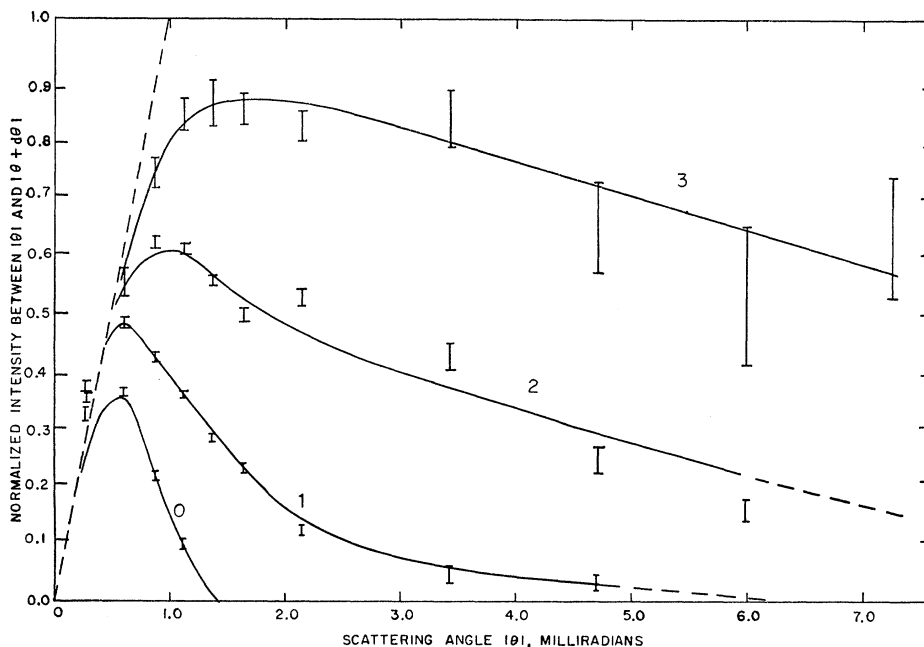


FIG. 13. Graphical estimate of the angular weighting factors for the spectrogram of Fig. 5, using the angular data of Fig. 9; the dashed line shows the asymptotic slope expected for all curves as $|\theta| \rightarrow 0$.

G. Interpretation

The value of $\lambda = 810 \pm 60$ Å, obtained from the spectrogram Fig. 10, is slightly higher than the limit of 560 Å reported by Blackstock, Ritchie, and Birkhoff² for a primary energy of 25 keV; however, as we have pointed out earlier, there are certain differences in the treatment of these data.

Two primary sources of systematic error remain in this measurement.

(a) *Treatment of the continuum.* If the method of subtracting continuum, used on Fig. 10, cannot be theoretically justified, this contributes a systematic error in the determination of t/λ which is larger than the statistical scatter in Fig. 12. In this respect, it may be suggested that the line shapes of Fig. 10 suggest a "natural line shape" for the single loss of Lorentzian form, which would contribute broad tails on the peaks for large N . A detailed investigation of this feature is in progress.

(b) *Neglect of large-angle scattering.* The method of observation for both the spectrogram of Fig. 5 and that of Fig. 10 excludes electrons scattered at angles greater than about 6 mrad. In Fig. 13 the first-loss curve is artificially truncated at 6 mrad; in practice, however, single inelastic scattering is known to continue out to a cutoff at about 18 or 20 mrad.^{5,6} Assuming a $1/\theta^2$ decay in the region between 6 and 20 mrad, as has recently been demonstrated by Kunz,⁵¹ this region of angle may be expected to contribute a total of <20% to the total cross section of Eq. (7). Hence the mean free path measured here is a mean free path for small-angle scattering ($\theta \leq 6 \times 10^{-3}$ rad) which may be up to 20% larger than the mean free path corresponding to the total cross section. Hence the discrepancy with the value of Blackstock, Ritchie, and Birkhoff may be partly a consequence of the incident angular distribution of Fig. 10 not being large enough to fully include the "tails" of the differential cross section. An experimental solution to this question is difficult to devise; if the data are to be recorded as a zero-angle spectrum with wide incident beam, as in Fig. 10, the incident beam must have a uniform angular distribution between -20×10^{-3} and $+20 \times 10^{-3}$ radian, a condition difficult to achieve in practice.

ACKNOWLEDGMENTS

The authors wish to thank the many colleagues who have contributed substantially to this work. The introductory discussion of inelastic scattering, and the treatment of the statistical data are due to U. Fano. Helpful and constructive criticism has been received from F. Lenz, R. Ferrell, H. Mendlowitz, and M. Berger. M. D. Wagner performed the observations shown in Fig. 6, while J. A. Suddeth suggested the problem of accommodation coefficient in the foil thickness measure-

ments. The computer program used in the calculation of the folding integrals was developed by L. Breed.

APPENDIX: CALCULATION OF THE FOLDING INTEGRALS

The calculation of folding integrals can be made by either of two methods: The functions to be folded may be replaced by their Fourier-Bessel transforms, and the inverse transform applied to the product of these (as indicated by Molière²² in his more general method of solution), or the functions may be evaluated and folded numerically. The first method has been used by Keil, Zeitler, and Zinn⁵² in their recomputation of Leisegang's results; it has the disadvantage of involving a full Fourier-Bessel transform for any numerical functions used, such as the zero-loss angular distribution measured in these experiments. Hence we have used the second method, which may be done by a computer program readily adapted to digest numerical input functions.

The method of integration has been as follows: the two functions to be folded are plotted (in full cylindrical symmetry) on fine-spaced x - y grids (spacing 0.25 mrad in Fig. 6, 0.20 mrad in Figs. 7 and 9). The two grids are overlaid, the functions are multiplied point-by-point, and the product values summed out to a cutoff radius of between 8 and 10 mrad. The sum is then taken as a single value of the integral function, whose argument is given by the separation between the maxima of the two functions. The maxima are then moved apart one grid space, and the calculation is repeated for the new value of argument. This operation has been programmed for the IBM 704 computer, using Fortran coding. Sample running time is 4 min/curve.

In cases where the experimentally-determined angular distributions are not wholly symmetrical about zero scattering angle (as is the case in Figs. 6 and 7) the positive and negative scattering angles have been treated as separate problems of cylindrical symmetry. In Fig. 9 the experimental symmetry is sufficient to allow the use of a common approximation function for positive and negative angles.

The value of θ_E used in the Ferrell differential cross section has been 0.350 mrad in Fig. 7 and 0.370 in Fig. 9, corresponding to ΔE of 14.0 and 14.8 eV, respectively. In Fig. 6 the positive-angle half of the first-loss curve has been evaluated with $\theta_E = 0.370$; the negative half, and the positive half of the second-loss curve have been evaluated with $\theta_E = 0.350$. Since it was not possible to measure ΔE with high accuracy during these angular measurements, these values were chosen to give best fit (0.350) to the experimental points, or to correspond to the widely quoted value of 14.8 eV (0.370) in the literature for this energy loss. The tail-width is particularly sensitive to this parameter.

⁵¹ C. Kunz (private communication).

⁵² F. Keil, E. Zeitler, and W. Zinn, Z. Naturforsch. **15a**, 1031 (1960).